Infinite Science Publishing

Proceedings Article

3D Trajectory Analysis for Tomographic Field Free Line Magnetic Particle Imaging

Damla Alptekin Soydan ⓘ*· Sefa Karaca ⓘ· Alper Güngör ⓘ· Can Barış Top ⓘ

ASELSAN Research Center, Aselsan A.Ş., Ankara, Turkey
*Corresponding author, email: dasoydan@aselsan.com.tr

Abstract

In magnetic particle imaging (MPI), spatial mapping of the magnetic nanoparticles is achieved by scanning the field-free region (FFR) throughout the field of view (FOV). The scanning trajectory of the FFR has an impact on image quality and scan time, and also is subject to limitations such as hardware requirements and patient safety. Here, we analyzed 3D imaging performance of an open-sided MPI system using simulations for various trajectories and SNR values. A selection field of $0.35\,\text{T}\,\text{m}^{-1}$ gradient with an FFL was created and scanned tomographically. For low SNR scenarios, the best imaging results were achieved at the expense of a longer scan time when 3D FOV was densely scanned layer by layer. For more sparse trajectories, the effect of the coherence between the scan angles became prominent with the increasing noise level. Image quality can be improved by assigning non-coherent FFL angles to the consequent layers while taking hardware limitations into account.

I. Introduction

In Magnetic particle imaging (MPI), the coils (or magnets) are configured to generate an inhomogeneous magnetic field with a field-free region (FFR), where the magnetic field strength is weak. By scanning the FFR inside the imaging volume, spatial mapping of the magnetic nanoparticles (MNP) is achieved. In cases where FFR is in the form of a line (field-free-line, FFL) larger regions are scanned faster with higher sensitivity [1]. Scanning of FFL through the field of view (FOV) can be performed by mechanical movements of the scanner or imaging specimen [2], or by the electronic movement of the FFL [3, 4], or a combination of both [5, 6]. Depending on the scanner design and the size of the imaging volume, FFL scan trajectories may differ from each other. Since the trajectory traversed by FFL has a significant impact on image quality and measurement duration, as well as patient safety and hardware requirements, the selection of an optimal trajectory is crucial.

In this study, we analyzed the 3D imaging results for different types of trajectories using a simulation model based on our in-house MPI system [7]. In previous studies, the imaging performance of the different types of trajectories were analyzed in a 2D scheme [8], and 3D simulations were conducted for slice-by-slice FFL scanning [9]. Here, the effect of different 3D trajectories on the imaging performance was analyzed at different SNR levels using system-matrix-based approach. In these analyses, the trajectories were investigated to achieve minimum scan time without averaging, rather than separating the effect of SNR and density for each trajectory.

II. Methods and Material

A selection field with an FFL was created using a bi-planar coil configuration in [7] (see Figure 1). The electronic rotation and translation of FFL were achieved by applying
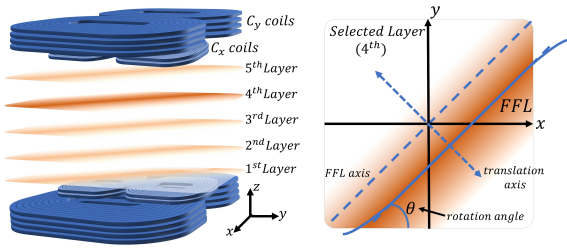
Figure 1: Open-sided MPI configuration. FFL can be generated at any arbitrary direction and scanned tomographically using C_x and C_y coils.
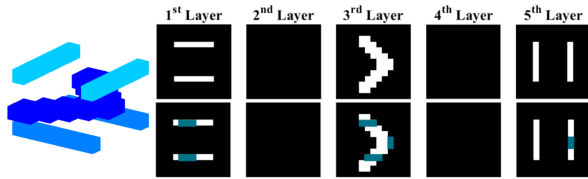

Figure 2: Designed 3D Phantom. The second and fourth layer were left empty. The highlighted parts of the phantoms at the bottom figure show the intersection of the nearest layer.

the following currents to the upper and lower coils:

$$
\begin{aligned}
I_{x,upper} &= c_x(z)\,I_{x_0}\cos(\theta)(1+\alpha_x(z)) \\
I_{x,lower} &= c_x(z)\,I_{x_0}\cos(\theta)(1-\alpha_x(z)) \\
I_{y,upper} &= c_y(z)\,I_{y_0}\sin(\theta)(1+\alpha_y(z)) \\
I_{y,lower} &= c_y(z)\,I_{y_0}\sin(\theta)(1-\alpha_y(z)).
\end{aligned}
\tag{1}
$$

In (1), I_{x_0} and I_{y_0} are the current values that form FFL with desired gradients in x- and y- directions, respectively. θ is the rotation angle of the FFL, $\alpha_i(z)$ is a coefficient to translate FFL in z-direction, $c_i(z)$ is a compensation factor to maintain the same gradient for any z- position in the imaging plane, and i indicates the coil type (x or y). Note that C_x and C_y coils (see Figure 1) generate a magnetic field in the z- direction, and FFL in x- and y- directions, respectively. After the translation of FFL to the corresponding layer, FFL was shifted in the xy-plane applying a drive field in z- direction.

For the numerical simulations, in-house MPI system [7] was modeled in *Matlab*. The gradient field efficiencies for C_x and C_y coils at the first and fifth layers were taken as 3.5 mT/m/A and 1.75 mT/m/A, respectively. An FFL with 0.35 T m^{-1} gradient was generated inside an imaging FOV of 52×52×20 mm^3, and discretized with 4×4×4 mm^3 cells. For each FFL angle, 25 cycles of drive field (9 mT peak, 25 kHz) was applied, and the received signal was sampled at 5 MS/s.

For image reconstruction, the frequency domain system matrix was filtered between 2-20 harmonics. The phantom in Figure 2 was reconstructed using the Alternating Direction Method of Multipliers (ADMM) method [7, 10].
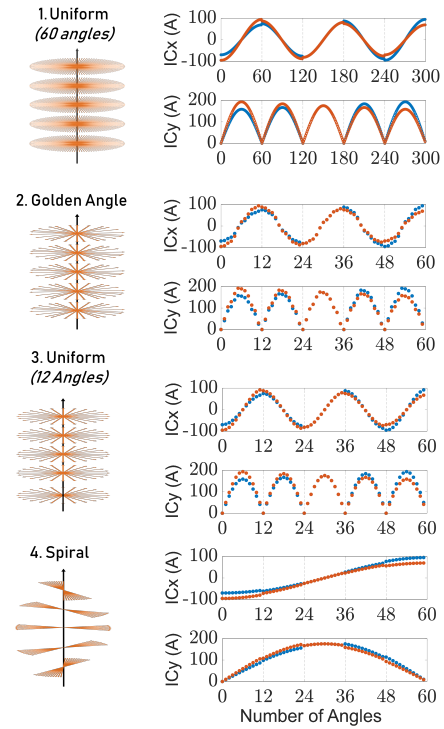

Figure 3: Analyzed trajectories and applied currents. In current diagrams, ICx and ICy correspond to applied currents to the C_x and C_y coils, respectively. Blue color represents the upper coils, whereas red color represents the lower coils.

Four 3D trajectories were analyzed: each layer was scanned with 1) 60 uniform FFL angles, 2) 12 golden-angles, 3) 12 uniform FFL angles, and 4) a spiral-like trajectory created using 12 consequent angles at each neighboring layer. For the first trajectory, the total number of angles was 300 (60 for each layer × 5), whereas for other trajectories 60 (12 for each layer × 5). For the second trajectory, golden-angles were rounded to the nearest angle with 3° resolution. The trajectories and corresponding applied currents are presented in Figure 3.

III. Results

Reconstructed images for different trajectories at various SNR levels are shown in Figure 4. For the low SNR scenario, the best imaging performance was achieved with the first trajectory due to the higher trajectory density (60 FFL angles at each layer) at the expense of a longer imaging time. Other trajectories employed 12 FFL angles at each layer, therefore scan duration corresponded to nearly one-fifth of the first trajectory.

The second and third scenarios showed similar imaging performance in terms of nRMSE, SSIM and visual inspection. The fourth trajectory, based on a slow variation of coil currents, resulted in poor imaging performance even for 30 dB SNR level because of the high coherence
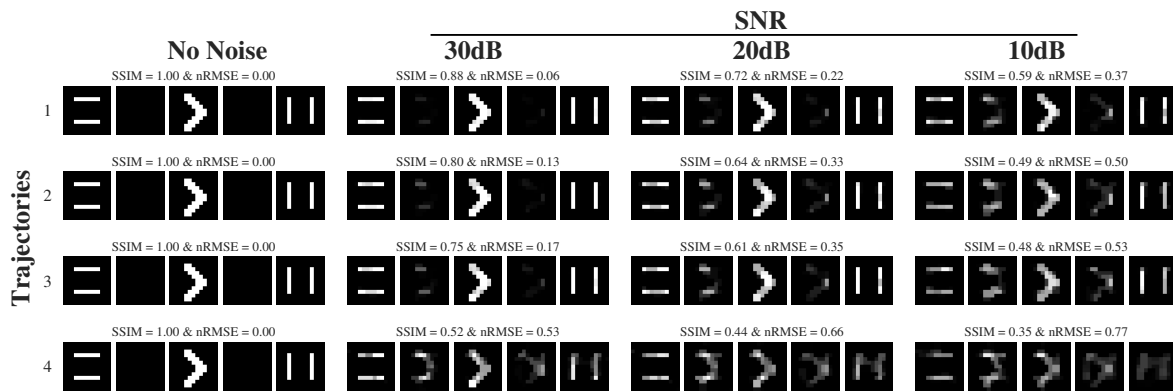
Figure 4: Reconstructed images. Trajectories: 1:Uniform - 60 angles, 2: Golden-angle, 3: Uniform - 12 angles, 4: Spiral
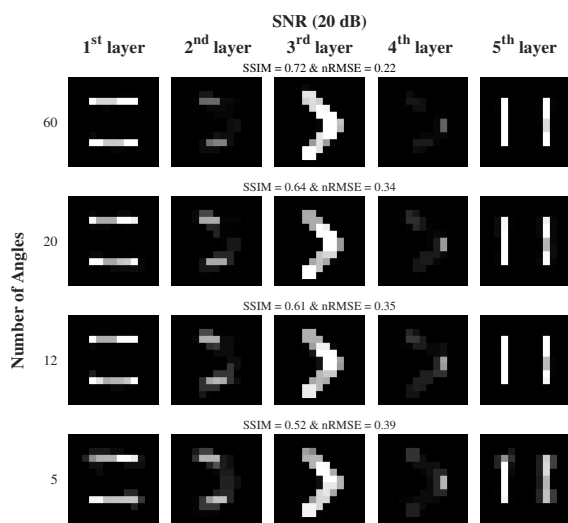

Figure 5: Reconstructed images at 20 dB SNR for uniformly distributed FFL angles at each layer.

IV. Conclusion

Overall, the results showed that there is a trade-off between scan duration and, image quality and hardware requirements. Decreasing the coherence between scan angles improves image quality; however, requires a faster transition from one FFL angle to the next, resulting in fast switching of coil currents. This is limited by the hardware specifications, i.e. requiring hardware with a high slew rate. The optimal trajectory should scan each layer with enough number angles for better reconstructions, and concurrently comply with hardware requirements. Here, a small FOV is analyzed using only selection and drive currents, further studies which include a focus coil for larger volume scanning should be studied further to optimize the imaging performance while taking the power and safety limitations into account.

Author's statement

Conflict of interest: Authors state no conflict of interest.

References

[1] P. W. Goodwill, J. J. Konkle, B. Zheng, E. U. Saritas, and S. M. Conolly. Projection x-space magnetic particle imaging. *IEEE Transactions on Medical Imaging*, 31(5):1076–1085, 2012.

[2] M. Weber, J. Beuke, A. Von Gladiss, K. Gräfe, P. Vogel, V. C. Behr, and T. M. Buzug. Novel Field Geometry Using Two Halbach Cylinders for FFL-MPI. *International Journal on Magnetic Particle Imaging*, Vol 4:No 2 (2018), 2019, Publisher: International Journal on Magnetic Particle Imaging. doi:10.18416/IJMPI.2018.1811004.

[3] K. Bente, M. Weber, M. Graeser, T. F. Sattel, M. Erbe, and T. M. Buzug. Electronic field free line rotation and relaxation deconvolution in magnetic particle imaging. *IEEE Transactions on Medical Imaging*, 34(2):644–651, 2015, doi:10.1109/TMI.2014.2364891.

[4] C. Greiner, M. A. Rückert, T. Kampf, V. C. Behr, and P. Vogel. Traveling Wave MPI utilizing a Field-Free Line. *International Journal on Magnetic Particle Imaging*, pp. Vol 8 No 1 Suppl 1 (2022), 2022, Publisher: International Journal on Magnetic Particle Imaging. (visited on 11/27/2022).

between the scan angles and partial sampling of the volume at each individual slice. On the other hand, due to the lower gradient strength, responsive MNPs from neighboring layers where FFL resides may have provided useful information for image reconstruction. Furthermore, this trajectory lightens the hardware requirements on slew rate since other trajectories require a fast variation of the coil currents, e.g., for the second scenario, the coil current change by 25 A to switch from one FFL angle to the next. In addition to the analyzed trajectories, the cases where scan angles are distributed uniformly for each layer were examined to show the effect of the number of FFL angles on the reconstructions (see Figure 5). Image quality deteriorated for a lower number of FFL angles, as expected. Note that, for all imaging trajectories, interlayer coupling artifacts were observed with increasing noise levels, and a low number of FFL angles. The highlighted parts of the phantom shown in Figure 2 caused artifacts to appear at the empty layers.

[5] J. J. Konkle, P. W. Goodwill, E. U. Saritas, and S. M. Conolly, Twenty-fold acquisition time improvement in 3d projection reconstruction mpi, in *2013 International Workshop on Magnetic Particle Imaging (IWMPI)*, 1–1, 2013. doi:10.1109/IWMPI.2013.6528322.

[6] E. Y. Yu, P. Chandrasekharan, R. Berzon, Z. W. Tay, X. Y. Zhou, A. P. Khandhar, R. M. Ferguson, S. J. Kemp, B. Zheng, P. W. Goodwill, M. F. Wendland, K. M. Krishnan, S. Behr, J. Carter, and S. M. Conolly. Magnetic particle imaging for highly sensitive, quantitative, and safe in vivo gut bleed detection in a murine model. *ACS Nano*, 11(12):12067–12076, 2017, PMID: 29165995. doi:10.1021/acsnano.7b04844.

[7] C. B. Top and A. Güngör. Tomographic field free line magnetic particle imaging with an open-sided scanner configuration. *IEEE Transactions on Medical Imaging*, 39(12):4164–4173, 2020, doi:10.1109/TMI.2020.3014197.

[8] C. B. Top, A. Güngör, S. Ilbey, and H. E. Güven. Trajectory analysis for field free line magnetic particle imaging. *Medical Physics*, 46(4):1592–1607, 2019, _eprint: https://aapm.onlinelibrary.wiley.com/doi/pdf/10.1002/mp.13411. doi:https://doi.org/10.1002/mp.13411.

[9] D. A. Soydan, A. Gungor, and C. B. Top, A Simulation Study for Three Dimensional Tomographic Field Free Line Magnetic Particle Imaging, in *2021 43rd Annual International Conference of the IEEE Engineering in Medicine & Biology Society (EMBC)*, 3701–3704, Mexico: IEEE, 2021. doi:10.1109/EMBC46164.2021.9631111.

[10] S. Ilbey, C. B. Top, A. Güngör, T. Çukur, E. U. Saritas, and H. E. Güven. Comparison of System-Matrix-Based and Projection-Based Reconstructions for Field Free Line Magnetic Particle Imaging. *International Journal on Magnetic Particle Imaging*, 3(1), 2017, doi:10.18416/ijmpi.2017.1703022.